

Optimal Control for Wind Turbine Wake Mixing on Floating Platforms

Maarten J. van den Broek * Daniel van den Berg 
Benjamin Sanderse ** Jan-Willem van Wingerden 

* *Delft Centre for Systems and Control, TU Delft, Delft,
The Netherlands (e-mail: m.j.vandenbroek@tudelft.nl)*

** *Scientific Computing, CWI, Amsterdam, The Netherlands*

Abstract: Dynamic induction control is a wind farm flow control strategy that utilises wind turbine thrust variations to accelerate breakdown of the aerodynamic wake and improve downstream turbine performance. However, when floating wind turbines are considered, additional dynamics and challenges appear that make optimal control difficult. In this work, we propose an adjoint optimisation framework for non-linear economic model-predictive control, which utilises a novel coupling of an existing aerodynamic wake model to floating platform hydrodynamics. Analysis of the frequency response for the coupled model shows that it is possible to achieve wind turbine thrust variations without inducing large motion of the rotor. Using economic model-predictive control, we find dynamic induction results that lead to an improvement of 7% over static induction control, where the dynamic controller stimulates wake breakdown with only small variations in rotor displacement. This novel model formulation provides a starting point for the adaptation of dynamic wind farm flow control strategies for floating wind turbines.

Keywords: non-linear predictive control, optimal control of hybrid systems, wind energy, floating wind turbines, wind farm control

1. INTRODUCTION

Offshore parcels suitable for fixed-bottom wind turbines are limited, leading to wind turbines being built in large, densely-spaced wind farms (van Wingerden et al., 2020). Floating wind turbines provide an opportunity to extend the suitable space for wind farm construction beyond shallow waters (i.e. deeper than 50 metres).

Wind farm flow control aims to reduce the negative effects of aerodynamic interaction between wind turbines in a farm with strategies such as wake redirection by yaw misalignment, induction control, and wake mixing strategies (Meyers et al., 2022). These control strategies have mostly been developed on fixed-bottom turbines. The implementation of wind farm flow control strategies for floating wind turbines requires specific attention as floating platforms introduce additional dynamics, instabilities, and resonant modes.

The current work focuses on dynamic induction control - the application of wind turbine thrust variations, and consequent induction variations, to stimulate breakdown of the aerodynamic wake behind the turbine. Optimal control studies with adjoint optimisation of large-eddy simulations (Goit and Meyers, 2015) provided the basis for

dynamic induction control signals, which, in a step towards practical application, have been reduced to sinusoidal thrust signals applied using collective pitch control. These have been found to improve wake recovery in a study with large-eddy simulations (Munters and Meyers, 2018) and in wind tunnel experiments (Frederik et al., 2020).

Recently, adjoint optimisation with a free-vortex wake representation of a wind turbine wake using a two-dimensional actuator-disc model has been used to find dynamic induction control signals in a non-linear economic model-predictive control setting (van den Broek et al., 2022). This study provided a cumbersome manual derivation of the discrete adjoint to enable gradient-based optimisation. It is computationally inexpensive compared to optimisation using large-eddy simulations.

The modelling of wake aerodynamics using free-vortex methods is suitable for adaptation to floating wind turbine platforms because the simulation uses Lagrangian particles, therefore allowing rotor motions without being limited by grid resolution and localised refinements. The wakes of floating wind turbines have previously been modelled using a free-vortex ring method (Dong et al., 2019) and free-vortex wake models have been used to study the wake dynamics (Lee and Lee, 2019). However, these studies focused on the performance of a single turbine instead of considering aerodynamic wake interaction.

To explore the possibilities for dynamic induction control on floating wind turbines, we extend the free-vortex wake model by van den Broek et al. (2022) with a floating platform model and utilise automatic differentiation to

* This work is part of the research programme “Robust closed-loop wake steering for large densely spaced wind farms” with project number 17512, which is (partly) financed by the Dutch Research Council (NWO). This project is part of the Floatech project. The research presented in this paper has received funding from the European Union’s Horizon 2020 research and innovation programme under grant agreement No. 101007142.

replace manual derivation of the discrete adjoint. The coupled aerodynamic and hydrodynamic model can then be used to explore optimal control of dynamic induction with gradient-based optimisation in an economic model-predictive control framework.

Contributions of this paper are: (i) extension of the free-vortex wake model with floating platform dynamics, (ii) implementation of the optimal control algorithm with automatic differentiation to avoid manual derivation of the adjoint, and (iii) exploration of wake mixing using optimal control for wind turbines on floating platforms.

The remainder of this paper is structured as follows. Section 2 describes the wake model for the floating wind turbine and methods for control optimisation. Section 3 discusses the results on wake mixing for floating platforms. Finally, conclusions are presented in Section 4.

2. MODELLING AND CONTROL

This section introduces the novel coupling of the aerodynamic wake model and hydrodynamic platform model for dynamic control optimisation. Section 2.1 describes, in brief, the use of the free-vortex wake to construct a 2D actuator-disc model for the representation of the wind turbine wake. The linear hydrodynamic model of a floating platform is presented in Section 2.2 and the connection to the aerodynamic model is described in Section 2.3. An objective function for mean power maximisation and receding horizon controller is defined in Section 2.4, such that optimal control signals may be explored in this novel framework.

2.1 Wind Turbine Wake Model

The free-vortex method is used to model the aerodynamic wake using a two-dimensional (2D) actuator-disc representation of a wind turbine. The basis of this model is presented in van den Broek et al. (2022). The vorticity formulation requires the assumption of inviscid and incompressible flow, although diffusion may be approximated. The actuator disc is assumed to be uniformly loaded so it only releases vorticity along its edge (Katz and Plotkin, 2001).

The 2D wake model in this work represents a horizontal slice (xy -plane) of the flow field at hub height. At every time step, pairs of vortex points are released from the edge of the rotor that travel downstream as Lagrangian markers. These vortex points are used to calculate the velocity deficit in the wake as illustrated in Figure 1.

The wake dynamics are modelled as a non-linear state-space system in discrete time for the state update at a time-step k ,

$$\mathbf{q}_{k+1} = f(\mathbf{q}_k, \mathbf{m}_k), \quad (1)$$

$$\mathbf{y}_k = g(\mathbf{q}_k, \mathbf{m}_k), \quad (2)$$

with the state vector $\mathbf{q} \in \mathbb{R}^{n_s}$, the control vector $\mathbf{m} \in \mathbb{R}^{n_c}$, and the output vector $\mathbf{y} \in \mathbb{R}^{n_t}$. The total number of states to describe the wake is n_s , the total number of controls is n_c and the number of turbines for which power output is estimated is n_t .

The velocity $\mathbf{u}_i \in \mathbb{R}^2$ induced at point $\mathbf{x}_0 \in \mathbb{R}^2$ by a single vortex element located at $\mathbf{x}_1 \in \mathbb{R}^2$, with vortex strength Γ , is calculated with the Biot-Savart law as

$$\mathbf{u}_i(\mathbf{x}_0, \mathbf{x}_1) = \begin{bmatrix} -r_y \\ r_x \end{bmatrix} \left(\frac{\Gamma}{2\pi} \frac{1}{\|\mathbf{r}\|^2} \right) \left(1 - \exp\left(-\frac{\|\mathbf{r}\|^2}{\sigma^2}\right) \right), \quad (3)$$

where the relative position \mathbf{r} is

$$\mathbf{r} = \mathbf{x}_1 - \mathbf{x}_0. \quad (4)$$

A Gaussian core with core size σ is included to regularise singular behaviour of the induced velocity close to the vortex element. The total velocity induced by all vortex elements is calculated by summation of all individual contributions. At every time step, a new set of vortex points is initialised at the edge of the rotor and all other points are propagated downstream.

The thrust T is calculated according to the mean velocity at the rotor plane \mathbf{u}_r ,

$$T = c'_t(a) \cdot \frac{1}{2} \rho A_r (\mathbf{n} \cdot \mathbf{u}_r)^2, \quad (5)$$

with local thrust coefficient c'_t , air density ρ , rotor swept area A_r and the rotor normal vector \mathbf{n} . Similarly, power P is calculated with the local power coefficient c'_p as

$$P = c'_p(a) \cdot \frac{1}{2} \rho A_r (\mathbf{n} \cdot \mathbf{u}_r)^3. \quad (6)$$

The thrust and power coefficient are a function of the induction factor a based on momentum theory,

$$c'_t(a) = \begin{cases} \frac{4a(1-a)}{(1-a)^2} = \frac{4a}{1-a} & \text{if } a \leq a_t, \\ \frac{c_{t1} - 4(\sqrt{c_{t1}-1})(1-a)}{(1-a)^2} & \text{if } a > a_t, \end{cases} \quad (7)$$

$$c'_p(a) = \frac{4a}{1-a}, \quad (8)$$

with the parameter $c_{t1} = 2.3$. The thrust coefficient calculation is based on momentum theory with a transition to a linear approximation for high induction values which is an empirical correction based on the Glauert correction (Burton et al., 2001).

For the performance estimate of virtual turbines, based on the velocity estimate without including their impact on the flow, the rotor velocity is lowered using the induction factor,

$$\mathbf{u}_r^* = (1-a)\mathbf{u}_r. \quad (9)$$

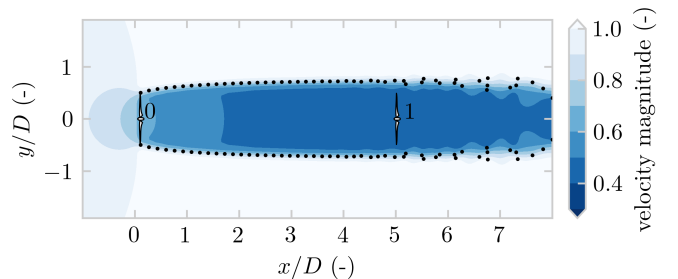


Fig. 1. Illustration of a flow field at hub height with the wind turbine wake for turbine 0, where turbine 1 at $x/D = 5$ downstream is modelled using the effective flow velocity. Units have been non-dimensionalised by rotor diameter and inflow velocity magnitude. The vortex points used for the velocity calculation are marked with black dots.

2.2 Floating Platform Model

The displacement of the rotor due to the dynamics of a floating base is calculated from platform motions in pitch (rotation along y) and surge (translation in x) degrees of freedom. These are the main motions influencing wind turbine thrust and power (Lee and Lee, 2019). The heave motion (translation in z) of the platform is neglected. The hydrodynamics of the platform motions are modelled using two decoupled mass-spring-damper systems, translational and rotational for surge and pitch, respectively. Figure 2 illustrates the model for the floating platform dynamics. The parameters used in this study are based on a triple-spar platform with a 10 MW reference turbine (Lemmer, 2018) and are listed in Table 1.

The assumption of linear platform hydrodynamics may be strong, but by neglecting non-linear hydrodynamics, we can put emphasis on the complexity of wake aerodynamics. Additionally, the tower and blades are assumed to be rigid. Decoupling of pitch and surge relies on assuming that translation happens at the centre of rotation. The tilt and

Table 1. Parameters for wind turbine, floating platform, and numerical configuration.

Rotor diameter	D	178.3 m
Nacelle height	h	119.0 m
Total mass	m_0	1.1×10^6 kg
Mass moment of inertia	$I_{yy,0}$	3.9×10^{10} kg m ²
Added mass	Δm	2.8×10^7 kg
Added inertia	ΔI_{yy}	1.1×10^{10} kg m ²
Pitch stiffness	k_ϕ	6.2×10^9 N m rad ⁻¹
Pitch damping	c_ϕ	7.3×10^8 N m s rad ⁻¹
Surge stiffness	k_x	8.3×10^4 N m ⁻¹
Surge damping	c_x	1.7×10^5 N s m ⁻¹
Time step - floater	Δt_f	0.9 s
Time step - wake	Δt_w	3.6 s
Number of rings	n_r	60
Vortex core size	σ	17.8 m
Air density	ρ	1.225 kg · m ³
Inflow velocity	u_∞	10.0 m s ⁻¹

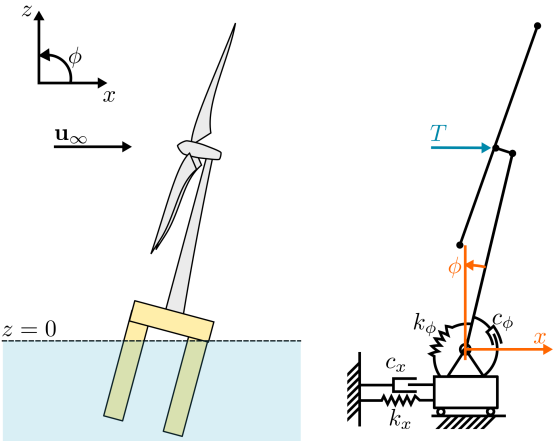


Fig. 2. Diagram of the simplified model for the dynamics of the floating wind turbine platform. Platform surge and pitch dynamics are modelled using, respectively, a translational and rotational mass-spring-damper system.

pitch angles are assumed small, and therefore the thrust is assumed aligned with the x -axis.

The equation of motion for platform pitch follows from a balance of moments around the centre of rotation,

$$I_{yy}\ddot{\phi} = -Th - k_\phi\phi - c_\phi\dot{\phi}, \quad (10)$$

with the mass moment of inertia I_{yy} , pitch angle ϕ , thrust T , tower height h , rotational hydrodynamic stiffness and damping k_ϕ and c_ϕ , respectively. The mass moment of inertia is the sum of physical inertia $I_{yy,0}$ and a hydrodynamic added inertia term ΔI_{yy} .

The equation of motion for surge follows from the balance of forces in x -direction,

$$m\ddot{x} = T - k_x x - c_x \dot{x}, \quad (11)$$

with total mass m , displacement of the centre of rotation x , and translational hydrodynamic stiffness and damping k_x and c_x , respectively. The total mass is the sum of physical mass m_0 and a hydrodynamic added mass term Δm .

Both equations of motion are put into a linear state-space form $\dot{\mathbf{x}} = \mathbf{A}\mathbf{x} + \mathbf{B}\mathbf{u}$ as

$$\begin{bmatrix} \dot{\phi} \\ \dot{\phi} \end{bmatrix} = \begin{bmatrix} 0 & 1 \\ -k_\phi/I_{yy} & -c_\phi/I_{yy} \end{bmatrix} \begin{bmatrix} \phi \\ \dot{\phi} \end{bmatrix} + \begin{bmatrix} 0 \\ -h/I_{yy} \end{bmatrix} T, \quad (12)$$

$$\begin{bmatrix} \dot{x} \\ \dot{x} \end{bmatrix} = \begin{bmatrix} 0 & 1 \\ -k_x/m & -c_x/m \end{bmatrix} \begin{bmatrix} x \\ \dot{x} \end{bmatrix} + \begin{bmatrix} 0 \\ 1/m \end{bmatrix} T. \quad (13)$$

These are converted to discrete-time state-space form using a zero-order hold with a time-step Δt_f for application in the numerical model framework according to

$$\mathbf{A}_d = \exp(\mathbf{A}\Delta t_f), \quad (14)$$

$$\mathbf{B}_d = \mathbf{A}^{-1}(\mathbf{A}_d - \mathbf{I})\mathbf{B}, \quad (15)$$

$$\mathbf{x}_{k+1} = \mathbf{A}_d\mathbf{x}_k + \mathbf{B}_dT. \quad (16)$$

2.3 Model Coupling

There exists a two-way coupling between the two models that is evaluated at every time step in the wake simulation. The thrust force is calculated from the difference between the effective wind speed and the motion of the rotor as calculated by the floating platform model. The position of the rotor from the floating platform model also specifies the position where the vortex points are released in the wake model.

The sampling time needs to be chosen such that dynamics at the natural frequency of the system are adequately captured. The resonant frequencies for the rigid floating platform are $\omega_\phi = 0.056$ Hz in the pitch and $\omega_x = 0.0085$ Hz in the surge degree of freedom. The sampling frequency of the wake model is insufficient to properly capture the floating dynamics for platform pitching motion. This is resolved by running the floater dynamics at a higher frequency, i.e. at a smaller time step $\Delta t_w = 4\Delta t_f$. The wake model is assumed to be constant during these smaller time steps for updating the thrust input to the floating platform dynamics.

Running the wake model at a higher sampling frequency is undesired because that would require equally more vortex points and more steps in the optimisation horizon. That quickly makes optimisation slow and cumbersome.

2.4 Control Optimisation

This work follows a non-linear economic model-predictive control (EMPC) approach for maximisation of mean power production as introduced in van den Broek et al. (2022) and briefly summarised here. Receding horizon control is implemented without terminal constraints by implementing a prediction horizon that is sufficiently long to remove the impact of finite horizon effects on the implemented control solution (Grüne, 2013).

The non-linear EMPC formulation requires optimisation of an objective function at every time step. We construct a scalar objective function $J : \mathbb{R}^{n_s n_c} \rightarrow \mathbb{R}$, that combines the output power for both turbines in \mathbf{y}_k and the change in control signal $\Delta \mathbf{m}_k = \mathbf{m}_k - \mathbf{m}_{k-1}$ as

$$J(\mathbf{q}_k, \mathbf{m}_k) = \mathbf{Q} \mathbf{y}_k + \Delta \mathbf{m}_k^T \mathbf{R} \Delta \mathbf{m}_k, \quad (17)$$

with output weight $\mathbf{Q} \in \mathbb{R}^{1 \times n_t}$ and input weight $\mathbf{R} \in \mathbb{R}^{n_c \times n_c}$. The output weight is chosen element-wise negative ($\mathbf{Q} < 0$) such that minimisation of the objective maximises mean power production and the input weight is chosen positive ($\mathbf{R} > 0$) to penalise actuation cost and smoothen the optimisation landscape. We then construct the unconstrained optimisation problem, subject to wake and platform dynamics, over a horizon of N_h steps, starting from step k_0 ,

$$\min_{\mathbf{m}_k} \sum_{k=k_0}^{k_0+N_h} J(\mathbf{q}_k, \mathbf{m}_k), \quad (18)$$

to find the optimal controls \mathbf{m}_k for $k \in [k_0; k_0 + N_h]$.

The optimisation problem is solved by using a gradient-based approach with the Adam optimiser using the default parameters (Kingma and Ba, 2015). The current work replaces the manual derivation of the adjoint equations by utilising reverse mode automatic differentiation with Zygote (Innes, 2018) to construct the gradient of the objective function.

3. RESULTS AND DISCUSSION

This section presents the optimal control signals and characterisation of system dynamics for the novel coupled model framework and receding horizon control strategy described in the previous section. A characterisation of the frequency response of the floating platform and wake aerodynamics is provided in Section 3.1. This is followed by a discussion of the results from the receding horizon optimisation of controls in Section 3.2.

3.1 Frequency Response

The frequency domain characteristics of the coupled wake and floating platform model are estimated by actuating the turbine induction with a chirp signal from 0.0025 Hz to 0.1 Hz over 30 000 s, with a mean value of $\bar{a} = 0.28$ and amplitude of $a = 0.05$. The FFT of the signals is used to estimate the frequency response functions. The estimation is performed for a floating platform with both pitch and surge degrees of freedom and for a single degree-of-freedom platform with either pitch or surge motion.

The response of wind turbine motion in response to dynamic induction variations is characterised by the response

in nacelle displacement in Figure 3. The resonance in surge and pitch modes of the platform motion appears as peaks in the magnitude of the tower top response. Actuation at these frequencies results in large motions of the rotor. There is a cross-over around $\omega^* = 0.02$ Hz where the combination of counter-phase pitch and surge motion results in a strongly reduced transmission to tower top displacement. This indicates the possibility for dynamic induction actuation on floating wind turbines with minimal movement of the rotor.

The effects of platform resonance also appear in the frequency response of turbine thrust to induction excitation as illustrated in Figure 4, when compared to a bottom-fixed turbine. The motion of the rotor on the floating platform reduces the effective thrust variation that can be achieved as resonant platform modes are excited. This reduction in thrust variation in response to the induction input is an important characteristic for finding optimal dy-

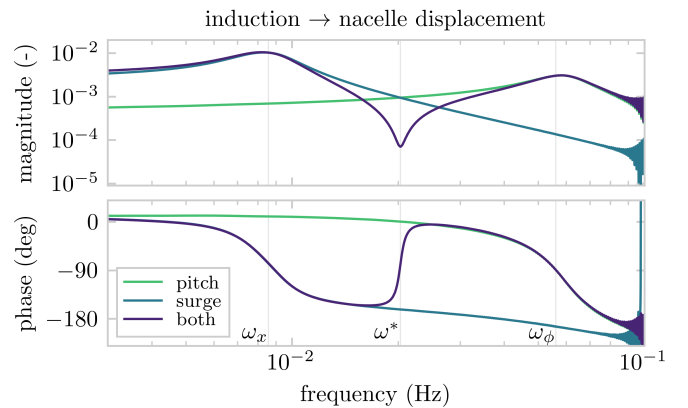


Fig. 3. Frequency response from induction excitation to tower top motion for different degrees of freedom of the floating platform. Resonance in the platform motion can be excited for both surge and pitch degrees of freedom resulting in large displacements at the rotor. However, the anti-resonant peak shows the two motions can combine to lead to a relatively stationary rotor while maintaining thrust variations.

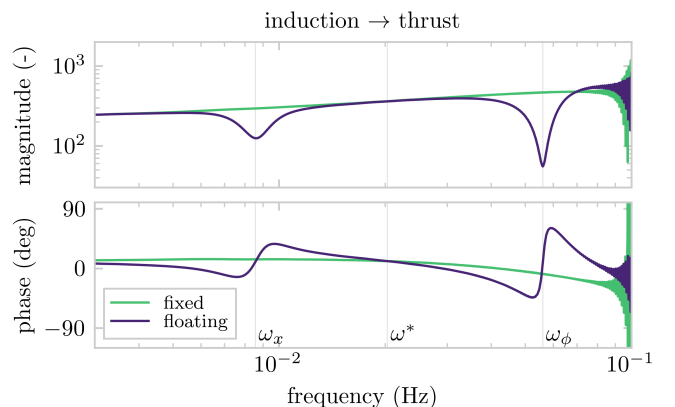


Fig. 4. Frequency response from induction excitation to turbine thrust for a bottom-fixed and floating wind turbine. Resonance in the platform motion for surge and pitch reduces the magnitude of thrust variations in response to induction input.

dynamic induction control signals on floating wind turbines. Reduced thrust variations consequently reduce the ability to stimulate breakdown of the wake.

We evaluate the effect of induction variations on turbine 0, with turbine 1 at its individual optimum, by taking a sinusoidal control signal that is slightly under-inductive,

$$a(t) = 0.28 + 0.05 \sin(2\pi ft), \quad (19)$$

and varying the frequency. The mean power is calculated once the simulation has converged to a quasi-steady state for every frequency. This stepped-frequency signal differs from the chirp signal in which this quasi-steady state for individual frequencies is not achieved. The resulting power characteristic is illustrated in Figure 5 for both fixed bottom turbines and for turbines on floating platforms.

For the illustrated sinusoidal sweep, the maximum mean power achieved is 10.92 MW for the fixed turbines and 10.90 MW for the turbines on floating platforms, at a frequency of 0.014 Hz and 0.016 Hz, respectively. These frequencies correspond to a dimensionless frequency of $St = 0.26$ and $St = 0.28$, which is close to the frequency found in previous results (Munters and Meyers, 2018; van den Broek et al., 2022). Dynamic induction actuation with a sinusoidal signal exceeds the maximum power production of 10.44 MW that could otherwise be achieved in this model with a static induction signal for both fixed and floating turbines.

The additional dynamics introduced by the floating platform appear slightly detrimental to the power that can be gained through thrust variations. The excitation of platform natural frequencies reduces the thrust variations that can be achieved and consequently the ability to excite the aerodynamic breakdown of the wake on floating platforms. Thrust variations can be achieved for frequencies in between the platform modes, especially those where the rotor is mostly stationary, i.e. the nacelle displacement due to induction variation is minimal.

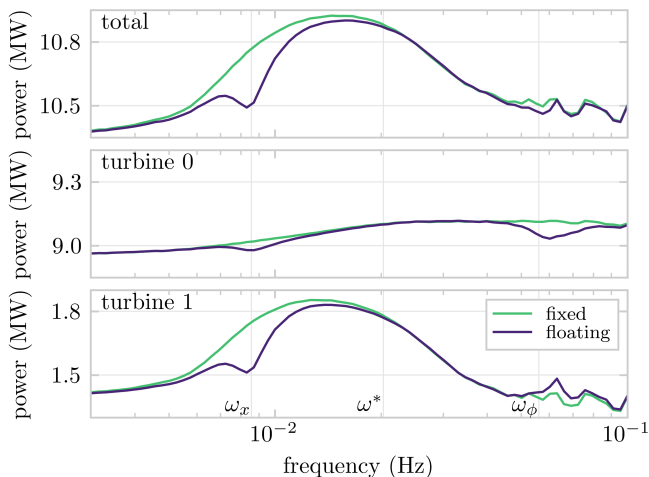


Fig. 5. Mean power production in quasi-steady state for dynamic induction excitation over frequency, comparing a simulation with a bottom-fixed turbine and a floating platform with pitch and surge degrees of freedom. Maximum power is produced at an actuation frequency of 0.014 Hz, which equals a Strouhal number of $St = 0.26$.

3.2 Economic Model-Predictive Control

The EMPC case study is run over 300 time steps, or 1080 s. As in van den Broek et al. (2022), the optimisation problem for control of turbine 0 is solved over a prediction horizon of $N_h = 100$ steps, equivalent to 360 s, and 50 optimiser iterations per step in the receding horizon. The objective weights $\mathbf{Q} = [-1 \ -1]$ MW⁻¹ and $\mathbf{R} = [4.7 \times 10^{-2}]$ are scaled to the physical problem. The first sample of the control solution is implemented as the simulation is advanced one time step, after which the control signal is shifted in time and re-optimised.

The dynamic induction control signal and power estimate found through the receding horizon optimisation of controls are illustrated in Figure 6, with the associated platform motions and nacelle displacement in Figure 7.

The control signal becomes roughly periodic after the transients have passed and the power estimate converges to a mean total power of 11.2 MW towards the end of the

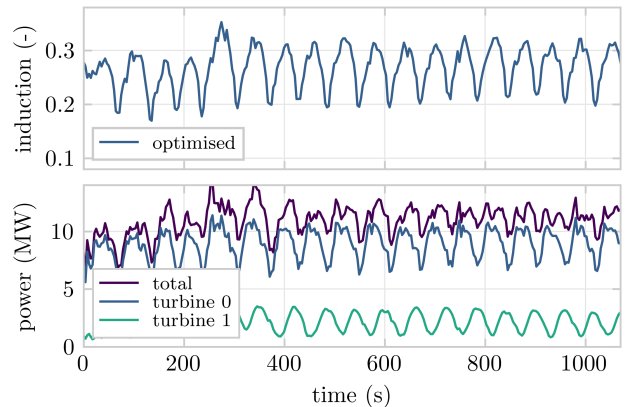


Fig. 6. The roughly periodic induction signal for turbine 0 is found through non-linear EMPC for maximisation of mean power production. The mean total power of 11.2 MW towards the end of the simulation is an improvement of 2.4% over the maximum with sinusoidal actuation shown in Figure 5.

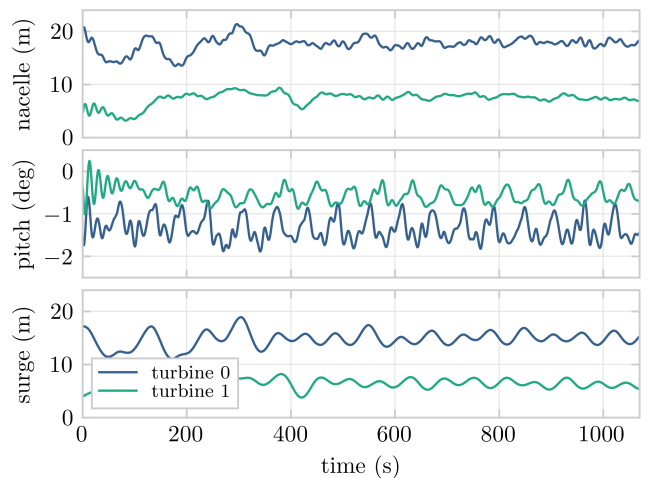


Fig. 7. The platform response associated with the control signal in Figure 6. Dynamic nacelle displacement is minimal and mostly driven by platform surge motion.

simulation. This is an improvement of 6.9% over what can be achieved with static induction control and 2.4% over the maximum with sinusoidal actuation shown in Figure 5. The associated nacelle displacement is relatively small, although the dynamic variation of induction, related to thrust, does trigger a response in the platform motions.

The frequency content associated with the induction signal is presented in Figure 6. The dominant frequency is 0.017 Hz ($St = 0.30$), which is close to the anti-resonance in the frequency response of the nacelle displacement (Figure 3). Dynamic induction excitation at this anti-resonant frequency allows large thrust variations to promote the aerodynamic breakdown of the wake while minimising rotor movement. The low sensitivity of upstream power to the precise frequency of thrust variation allows the optimisation space to find the optimal excitation frequency.

This excitation happens at significantly higher frequency than the $St = 0.20$ found by van den Broek et al. (2022) with the same model formulation, but for fixed-bottom turbines. This indicates the significant impact of the floating platform on the wind farm flow control strategy. It is important to note that the optimal frequency for aerodynamic excitation of wake breakdown should not be too close to the resonant frequencies for platform motion. The large displacement of the rotor would then lead to large power losses at the upstream turbine and limit the possibilities for stimulation of wake mixing due to loss of thrust variation.

4. CONCLUSION

The work presented in this paper provides a novel hybrid model-based approach for the optimisation of dynamic induction control signals for wind turbines on floating platforms to stimulate wake breakdown and improve mean power production under waked conditions.

A 2D free-vortex wake representation of the wind turbine wake using an actuator-disc model is coupled with a floating platform model with pitch and surge degrees of freedom. The exploration of the frequency response of the coupled wake and floating platform model shows that platform motions may lead to reduced thrust variations for dynamic induction control. On the other hand, platform motions may also combine to allow large thrust variations with minimal rotor movement. The control signal found

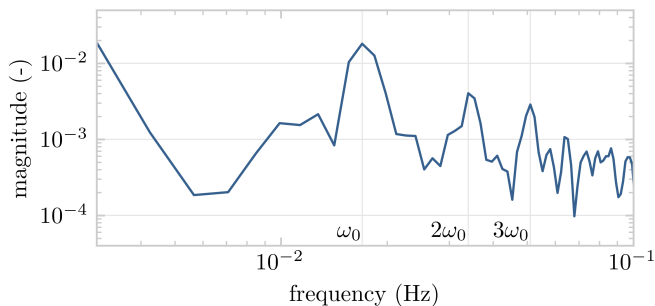


Fig. 8. The frequency content for the induction signal from Figure 6 has a peak at $\omega_0 = 0.017$ Hz and several harmonics. The dominant peak is close to the frequency of 0.02 Hz where transmission to tower top motion is minimal.

in the non-linear EMPC demonstrates dynamic induction control for wind turbines on a floating platform, effectively stimulating aerodynamic wake breakdown without inducing large displacements of the rotor.

Future work may explore validation with higher fidelity models or a co-design approach to simultaneously adapt platform parameters and control signals to improve dynamic control performance.

REFERENCES

- Burton, T., Sharpe, D., Jenkins, N., and Bossanyi, E. (2001). *Wind Energy Handbook*. Wiley.
- Dong, J., Viré, A., Ferreira, C.S., Li, Z., and Van Bussel, G. (2019). A modified free wake vortex ring method for horizontal-axis wind turbines. *Energies*, 12(20), 1–24. doi:10.3390/en12203900.
- Frederik, J.A., Weber, R., Cacciola, S., Campagnolo, F., Croce, A., Bottasso, C., and van Wingerden, J.W. (2020). Periodic dynamic induction control of wind farms: Proving the potential in simulations and wind tunnel experiments. *Wind Energy Sci.*, 5(1), 245–257. doi:10.5194/wes-5-245-2020.
- Goit, J.P. and Meyers, J. (2015). Optimal control of energy extraction in wind-farm boundary layers. *J. Fluid Mech.*, 768, 5–50. doi:10.1017/jfm.2015.70.
- Grüne, L. (2013). Economic receding horizon control without terminal constraints. *Automatica*, 49(3), 725–734. doi:10.1016/j.automatica.2012.12.003.
- Innes, M. (2018). Don’t unroll adjoint: Differentiating ssa-form programs. doi:10.48550/arxiv.1810.07951.
- Katz, J. and Plotkin, A. (2001). *Low-Speed Aerodynamics*. Cambridge University Press, 2 edition.
- Kingma, D.P. and Ba, J.L. (2015). Adam: A method for stochastic optimization. *3rd Int. Conf. Learn. Represent. ICLR 2015 - Conf. Track Proc.*, 1–15.
- Lee, H. and Lee, D.J. (2019). Effects of platform motions on aerodynamic performance and unsteady wake evolution of a floating offshore wind turbine. *Renew. Energy*, 143, 9–23. doi:10.1016/j.renene.2019.04.134.
- Lemmer, F. (2018). *Low-Order Modeling, Controller Design and Optimization of Floating Offshore Wind Turbines*. Ph.D. thesis.
- Meyers, J., Bottasso, C., Dykes, K., Fleming, P., Gebraad, P., Giebel, G., Göçmen, T., and van Wingerden, J.W. (2022). Wind farm flow control: prospects and challenges. *Wind Energy Sci. Discuss.*, (March), 1–55. doi:10.5194/wes-2022-24.
- Munters, W. and Meyers, J. (2018). Towards practical dynamic induction control of wind farms: Analysis of optimally controlled wind-farm boundary layers and sinusoidal induction control of first-row turbines. *Wind Energy Sci.*, 3(1), 409–425. doi:10.5194/wes-3-409-2018.
- van den Broek, M.J., De Tavernier, D., Sanderse, B., and van Wingerden, J.W. (2022). Adjoint optimisation for wind farm flow control with a free-vortex wake model. doi:10.48550/arxiv.2208.11516.
- van Wingerden, J.W., Fleming, P.A., Göçmen, T., Eguinoa, I., Doekemeijer, B.M., Dykes, K., Lawson, M., Simley, E., King, J., Astrain, D., Iribas, M., Bottasso, C.L., Meyers, J., Raach, S., Kölle, K., and Giebel, G. (2020). Expert Elicitation on Wind Farm Control. *J. Phys. Conf. Ser.*, 1618(2). doi:10.1088/1742-6596/1618/2/022025.